

Modelling and Simulation of a Continuous Facesheet MEMS Deformable Mirror

Curtis R. Vogel and Qiang Yang

*Department of Mathematical Sciences, Montana State University
Bozeman, MT 59717-2400*

vogel@math.montana.edu, yang@math.montana.edu

We introduce a coupled system of nonlinear partial differential equations (PDEs) to model a particular MEMS deformable mirror consisting of a continuous facesheet coupled with electrostatic plate-driven actuators. To make the problem computationally tractable, we reduced the system to a single linear PDE for the facesheet coupled with nonlinear algebraic constraints for each of the actuators. The resulting system is then solved numerically. Simulation results are presented. © 2005 Optical Society of America

OCIS codes: 010.1080,230.4040,230.3990

1. Introduction

This paper is motivated in part by the goal of achieving open-loop control of deformable mirrors (DMs) in adaptive optics (AO) systems. Very high resolution open-loop control is a requirement for advanced AO concepts for future giant telescopes like multi-object AO.¹ One of the prerequisites for open-loop DM control is a very accurate description of the response of the DM to the voltage inputs. Previous attempts have been made to develop accurate models for conventional piezostack actuated DMs.^{2,3}

In this paper we address the modelling of certain DMs which utilize micro-electro-mechanical systems (MEMS) technology. In particular, we focus on a MEMS device developed by Boston Micromachines Corporation (BMC)^{4,5,6,7} which consists of electrostatically driven actuators coupled to a continuous facesheet via rigid posts. See Fig. 1.

BMC's MEMS device offers a number of advantages over other designs. Unlike segmented MEMS DMs, the continuous facesheet does not scatter light. This makes it suitable for extremely high resolution AO (ExAO) applications like exoplanet detection.⁸ This device is also nonhysteretic—an attribute that greatly simplifies the modelling and should help facilitate open-loop control. Finally, the components of the BMC MEMS device are well-understood and are relatively easy to model. The deformations of the facesheet under known actuator

loading can be obtained by solving a linear fourth order partial differential equation (PDE) known as the plate equation, or two-dimensional biharmonic equation.⁹ Each actuator, which consist of a plate composed of semiconducting material suspended above a silicon substrate, can also be modelled using the plate equation; see Bifano et al.⁴ However, due to the inverse square law for electrostatic potential, there is a loading term in the actuator PDE model of Bifano et al that depends on the displacement in a nonlinear manner.

To carry out our modelling effort, we first extend the Bifano actuator model to account for the loading due to the rigid post and then combine it with the plate equation model for the facesheet. This results in a coupled system of $n_a + 1$ fourth order PDEs, where n_a denotes the number of actuators. Only the facesheet PDE is linear; the n_a actuator PDEs are nonlinear. To make this system computationally tractable, we replace each of the n_a actuator PDEs by nonlinear algebraic equations. This step is facilitated by the fact that actuator voltage and actuator plate loading due to the rigid post uniquely determine the actuator displacement at the location of the post. The end result is a single fourth order linear PDE coupled with n_a algebraic equations. This system can then be solved in a relatively straightforward manner using a finite element discretization combined with a Newton iteration to handle the nonlinearity.

This paper is organized as follows. Section 2 contains a detailed description of the coupled system of fourth order PDE boundary value problems which constitute the MEMS model. We then apply changes of variables to reduce the system of PDEs to nondimensional form. This reduces the number of parameters in the actuator model from seven to two. An additional nondimensional parameter arises from the actuator-to-facesheet coupling. In section 3a we reduce the PDE for each actuator to a nonlinear algebraic equation. In section 3b we outline the numerical solution of the resulting system, which consists of single PDE with algebraic constraints. Section 4 contains simulation results. Finally, we present conclusions in Section 5.

2. The Mathematical Model

For simplicity of presentation, unless otherwise specified, we assume that model parameters are constants. The deformation w of the facesheet at position $\mathbf{x} = (x, y)$ is modelled as the solution to the plate, or biharmonic, equation with point loading,

$$D_{\text{fs}} \nabla^4 w = - \sum_{i=1}^{n_a} p_i \delta(\mathbf{x} - \mathbf{x}_i), \quad (1)$$

on an $L \times L$ square with free boundary conditions. The \mathbf{x}_i denote the actuator post locations, p_i denotes the point load due to the actuator post, δ denotes the Dirac delta, D_{fs} denotes the flexural rigidity of the facesheet, n_a is the number of actuators, and the two-dimensional

biharmonic operator is defined by

$$\nabla^4 w \stackrel{\text{def}}{=} \frac{\partial^4 w}{\partial x^4} + 2 \frac{\partial^4 w}{\partial x^2 \partial y^2} + \frac{\partial^4 w}{\partial y^4}. \quad (2)$$

The displacement $z_i(\mathbf{x}')$ of the i th actuator plate satisfies

$$D_a \nabla^4 z_i = p_i \delta(\mathbf{x}' - \mathbf{0}) + \frac{\epsilon_0 \epsilon_r V_i^2}{(g - z_i(\mathbf{x}'))^2}. \quad (3)$$

Here \mathbf{x}' gives location in a local coordinate system for a square of dimensions $\ell \times \ell$, centered at the origin $\mathbf{0}$. Local coordinate position $\mathbf{0}$, the location of the actuator post, corresponds to location \mathbf{x}_i in the facesheet coordinate system. Two opposite edges of the actuator plate are clamped, while the other two edges are free. p_i is again the point load due to the post, but with opposite sign from eqn (1), D_a is the flexural rigidity of the actuator plate, ϵ_0 is the permittivity of free space, ϵ_r is dielectric constant of the gap media, g is the gap size of the actuator, and V_i is the applied voltage. In addition, the actuator displacements must match the facesheet displacements at the posts, so

$$w(\mathbf{x}_i) = z_i(\mathbf{0}), \quad i = 1, \dots, n_a. \quad (4)$$

To convert eqn (3) to nondimensional form, we apply the change of variables

$$\tilde{z}_i = z_i/g, \quad \tilde{\mathbf{x}}' = \mathbf{x}'/\ell. \quad (5)$$

This yields

$$\nabla^4 \tilde{z}_i = \rho_i \delta(\tilde{\mathbf{x}}' - \mathbf{0}) + \frac{\nu_i}{(1 - \tilde{z}_i(\tilde{\mathbf{x}}'))^2}, \quad (6)$$

where

$$\rho_i = \frac{\ell^4 p_i}{g D_a}, \quad (7)$$

$$\nu_i = \frac{\epsilon_0 \epsilon_r \ell^4 V_i^2}{g^3 D_a} \quad (8)$$

Similarly, the change of variables

$$\tilde{w} = w/g, \quad \tilde{x} = x/L, \quad (9)$$

when applied to eqn (1), yields

$$\nabla^4 \tilde{w} + \sigma \sum_{i=1}^{n_a} \rho_i \delta(\tilde{\mathbf{x}} - \tilde{\mathbf{x}}_i) = 0, \quad (10)$$

where

$$\sigma = \left(\frac{L}{\ell}\right)^4 \frac{D_a}{D_{\text{fs}}}. \quad (11)$$

The constraint (4) becomes

$$\tilde{w}(\tilde{\mathbf{x}}_i) = \tilde{z}_i(\mathbf{0}), \quad i = 1, \dots, n_a. \quad (12)$$

For notational simplicity, we now drop the over-tilde ($\tilde{\cdot}$) from the variables in (5)-(12).

3. Solution Techniques

3.A. Model Reduction

To make the system (6), (10), (12) computationally tractable, we first apply a nonlinear finite element solver to the nonlinear PDE (6) to obtain the actuator plate displacement. For notational simplicity, we drop the subscript i from variables in the discussion in this paragraph. Figure 2 shows two solutions $z(\mathbf{x}; \rho, \nu)$ to eqn (6), corresponding to two of different parameter vectors (ρ, ν) . Although the parameter ν (proportional to square of the applied voltage) is the same in both cases, the parameter ρ (proportional to load due to the post) is positive in one case and negative in the second case. This results in very different qualitative behaviors in the actuator plate displacements in the two cases.

We next evaluate z at the post location $\mathbf{0}$. Fig. 3 shows how $z(\mathbf{0}; \rho, \nu)$ varies with parameters ρ and ν . Given a functional relationship $z(\mathbf{0}; \rho, \nu) = f(\rho, \eta)$, we apply the constraint (12) and combine it with the facesheet model equation (10) to obtain the system

$$\nabla^4 w + \sigma \sum_{i=1}^{n_a} \rho_i \delta(\mathbf{x} - \mathbf{x}_i) = 0, \quad (13)$$

$$w(\mathbf{x}_i) = f(\rho_i, \nu_i), \quad i = 1, \dots, n_a. \quad (14)$$

Note that we are assuming actuator uniformity in the algebraic constraints (14). If the actuators were nonuniform, e.g., if the gap size or electromechanical properties varied between actuators, then we would need to replace the single function f with a different function f_i for each actuator.

3.B. Solution to the Reduced System

Eqn (13)-(14) constitute a single fourth order linear PDE with n_a algebraic constraints. To solve this system we first apply a standard Galerkin finite element discretization to the PDE.¹⁰ This means we assume an expansion

$$w(\mathbf{x}) = \sum_{k=1}^N w_k b_k(\mathbf{x}), \quad (15)$$

we substitute this expansion into the PDE (13), we multiply both sides of (13) by $b_j(\mathbf{x})$, we integrate over the unit square. Applying integration by parts to the left hand side and suppressing boundary terms, we obtain

$$\sum_{k=1}^N \left(\int \nabla^2 b_j \nabla^2 b_k d\mathbf{x} \right) w_k + \sigma \sum_{i=1}^{n_a} \rho_i b_j(\mathbf{x}_i) = 0, \quad j = 1, \dots, N. \quad (16)$$

Substituting the expansion (15) into (14) gives

$$\sum_{k=1}^N w_k b_k(\mathbf{x}_i) = f(\rho_i, \nu_i), \quad i = 1, \dots, n_a. \quad (17)$$

The discretized system (16)-(17) can be expressed as

$$\mathbf{G}(\mathbf{w}, \boldsymbol{\rho}) = \begin{bmatrix} \mathbf{G}_1(\mathbf{w}, \boldsymbol{\rho}) \\ \mathbf{G}_2(\mathbf{w}, \boldsymbol{\rho}) \end{bmatrix} \stackrel{\text{def}}{=} \begin{bmatrix} A\mathbf{w} + \sigma B\boldsymbol{\rho} \\ B^T\mathbf{w} - \mathbf{f}(\boldsymbol{\rho}, \boldsymbol{\nu}) \end{bmatrix} = \begin{bmatrix} \mathbf{0} \\ \mathbf{0} \end{bmatrix}. \quad (18)$$

Here the ‘‘stiffness matrix’’ A has jk -th element given by the coefficient of w_k in the first term in eqn (16). The matrix B has entries

$$B_{ji} = b_j(\mathbf{x}_i), \quad j = 1, \dots, N, \quad i = 1, \dots, n_a. \quad (19)$$

We use tensor products of cubic Hermite splines as the expansion functions $b_k(\mathbf{x})$ in eqn (15). Hence both A and B are sparse matrices. In addition, A is positive semi-definite, with a 3-dimensional null space consisting of discretized piston (constant function), and tip-tilt (linear functions in x and y).

The discrete system (18) is nonlinear due to the nonlinear function \mathbf{f} . To solve this system we apply the Newton iteration

$$(\mathbf{w}_{k+1}, \boldsymbol{\rho}_{k+1}) = (\mathbf{w}_k, \boldsymbol{\rho}_k) - \mathbf{G}'(\mathbf{w}_k, \boldsymbol{\rho}_k)^{-1} \mathbf{G}(\mathbf{w}_k, \boldsymbol{\rho}_k), \quad k = 0, 1, \dots \quad (20)$$

Here k is the iteration index, $(\mathbf{w}_0, \boldsymbol{\rho}_0)$ is an initial guess, and the derivative of \mathbf{G} is given by

$$\mathbf{G}'(\mathbf{w}, \boldsymbol{\rho}) = \begin{bmatrix} A & \sigma B \\ B^T & -D \end{bmatrix}. \quad (21)$$

From the right hand side of (17), D is an $n_a \times n_a$ diagonal matrix with diagonal entries

$$[D]_{ii} = \frac{\partial f}{\partial \rho_i}, \quad i = 1, \dots, n_a. \quad (22)$$

The computation of the Newton step in (20), $(\Delta \mathbf{w}_k, \Delta \boldsymbol{\rho}_k) \stackrel{\text{def}}{=} -\mathbf{G}'(\mathbf{w}_k, \boldsymbol{\rho}_k)^{-1} \mathbf{G}(\mathbf{w}_k, \boldsymbol{\rho}_k)$, requires solution of the linear system

$$\begin{bmatrix} A & \sigma B \\ B^T & -D \end{bmatrix} \begin{bmatrix} \Delta \mathbf{w} \\ \Delta \boldsymbol{\rho} \end{bmatrix} = \begin{bmatrix} -\mathbf{G}_1 \\ -\mathbf{G}_2 \end{bmatrix}, \quad (23)$$

where \mathbf{G}_1 and \mathbf{G}_2 are given in (18). Using the equation defined by the second block row in (23), we can solve for $\Delta \boldsymbol{\rho}$ in terms of $\Delta \mathbf{w}$,

$$\Delta \boldsymbol{\rho} = D^{-1}(B^T \Delta \mathbf{w} + \mathbf{G}_2) \quad (24)$$

and substitute into the equation for the first block row to obtain

$$(A + \sigma B D^{-1} B^T) \Delta \mathbf{w} = -\mathbf{G}_1 - \sigma B D^{-1} \mathbf{G}_2. \quad (25)$$

By solving this linear system we obtain $\Delta \mathbf{w}_k$. We then compute $\Delta \boldsymbol{\rho}_k$ using (24).

Note that \mathbf{G}_1 , \mathbf{G}_2 , and D may all vary with iteration, while A and B remain fixed. In addition, $A + \sigma BD^{-1}B^T$ is symmetric positive definite (SPD) and with finite element discretization it is sparse. Hence specialized techniques for sparse SPD matrices¹¹ like the preconditioned conjugate gradient method may be applied to efficiently solve (25) when the number of actuators is large. Finally, since D is diagonal, computation of $\Delta \boldsymbol{\rho}$ via (24) is trivial.

4. Simulation Results

We now apply the results of the previous sections to investigate the behavior of a simulated MEMS DM with 64 actuators distributed on an equispaced 8×8 grid. In what follows, facesheet displacement is measured relative to actuator gap size; see eqn (9). Recall that the parameter ν_i is proportional to the square of the voltage applied to the i th actuator; see eqn (8). As in the previous sections, we shall assume that actuators respond uniformly to a given applied voltage and post loading. Hence, when the same voltage is applied to all the actuators, the facesheet displacement will be a constant, known as piston, which is independent of location \mathbf{x} but varies with squared voltage. Fig. 4 shows that for small values of $\nu = \nu_i$, piston depends linearly on ν . Once the piston exceeds about 10 percent of gap size, this dependence becomes nonlinear. The Newton iteration (20) fails to converge as piston approaches 30 percent of gap size. This corresponds to a MEMS device failure known as snap-down, in which the electrostatic force on an actuator plate becomes so large that the plate is pulled down to the base.

We next investigate the behavior of the model as we “poke”, or apply voltage to, adjacent actuators. We select a “bias”, or voltage applied uniformly to all the actuators, so that the constant facesheet displacement, or piston bias, w_{bias} is about 13 percent of the gap size. We then apply a positive poke to a central actuator. By this we mean the difference between applied voltage and the bias is positive. Let $\nu_{\text{bias}} = 40$ and $\nu_1 = 68$, respectively, denote the values of the parameter ν (see eqn (8)) corresponding to the bias voltage and the positive poke voltage. Fig. 5a provides a mesh plot of the resulting facesheet displacement, which we denote by $w_1(x, y)$, and Fig 5b shows a cross-section.

We next apply the same voltage pattern to a second, adjacent, actuator ($\nu_{\text{bias}} = 40$, $\nu_2 = 68$), and we denote the resulting displacement by $w_2(x, y)$. Note that w_2 has the same appearance as w_1 , but is shifted to the right by one actuator. By the *differential displacements* we mean the difference between the displacements and the bias,

$$\Delta w_i(x, y) \stackrel{\text{def}}{=} w_i(x, y) - w_{\text{bias}}, \quad i = 1, 2. \quad (26)$$

A cross-section of the sum of the differential displacements, $\Delta w_1(x, y) + \Delta w_2(x, y)$, appears as the dotted curve in Fig. 5c. We also simultaneously poked both the actuators with the same

voltages, taking $\nu_1 = \nu_2 = 68$ and applying the same bias $\nu_{\text{bias}} = 40$ as before. We denote the resulting facesheet displacement by $w_{12}(x, y)$. The cross-section of the corresponding differential displacement, $\Delta w_{12}(x, y) \stackrel{\text{def}}{=} w_{12}(x, y) - w_{\text{bias}}$, is plotted as the solid curve in Fig. 5c. Note that the peak value of Δw_{12} (solid curve) is more than 15 percent larger than the peak value of $\Delta w_1 + \Delta w_2$ (dashed curve). This clearly shows that the differential displacements do not depend on actuator voltage in an additive manner. It should be noted that then the differential displacements do become much more nearly additive as the applied voltages become much smaller.

5. Conclusions

In this paper we introduced a mathematical model, based on a system of PDEs which are derived from basic physical principles, for a MEMS DM consisting of a continuous facesheet coupled with electrostatic plate-driven actuators. We nondimensionalized the model equations, thereby reducing the number of model parameters from seven to three. To facilitate efficient numerical solution, we reduced the system to a single linear PDE for the facesheet with nonlinear algebraic constraints for each actuator. We then combine Finite Element discretization with Newton’s method to handle the nonlinearities and with sparse solution techniques to solve the resulting large linear systems.

Using the numerical tools we developed, we simulated a MEMS DM. We found that when large voltages were applied to adjacent actuators, the response of the simulated device was clearly non-additive.

6. Acknowledgement

This work has been supported in part by the Computational Mathematics Program at the Air Force Office of Scientific Research through AFOSR-DEPSCoR grant F49620-02-1-0297.

References

1. R. Dekany, M. Britton, D. Gavel, B. L. Ellerbroek, G. Herriot, C. Max, and J.-P. Veran, “Adaptive optics requirements definition for TMT”, in *Advances in Adaptive Optics*, edited by D. B. Calia, B. L. Ellerbroek, and R. Ragazzoni, Proc. SPIE **5490**, pp. 879–890 (2004).
2. C. L. Hom, P. D. Dean, and S. R. Winzer, “Simulating electrostrictive deformable mirrors: I. Nonlinear static analysis”, *Smart Mater. Struct.* **8** (1999), pp. 691–699.
3. C. L. Hom, P. D. Dean, and S. R. Winzer, “Simulating electrostrictive deformable mirrors: II. Nonlinear dynamic analysis”, *Smart Mater. Struct.* **8** (1999), pp. 700–708.

4. T. G. Bifano, R. K. Mali, J. K. Dorton, J. Perreault, N. Vandelli, M. N. Horenstein, D. A. Castanon, "Continuous-membrane surface-micromachined silicon deformable mirror," *Opt. Eng.* **36**(5), 1354–1360 (1997).
5. R. K. Mali, N. Vandelli, M. N. Horenstein, "Development of microelectromechanical deformable mirrors for phase modulation of light," *Opt. Eng.* **36**(2), 542–548 (1997).
6. T. G. Bifano, J. Perreault, P. Bierden, and C. Dimas, "Micromachined deformable mirrors for adaptive optics," *High-resolution wavefront control: methods, devices and applications IV*, edited by J. D. Gonglewski, M. A. Vorontsov, M. T. Gruneisen, S. R. Restaino, R. K. Tyson, *Proc. SPIE* **4825**, 10-13 (2002).
7. J. Perreault, T. G. Bifano, B. M. Levine, M. N. Horenstein, "Adaptive optics correction using microelectromechanical deformable mirrors," *Opt. Eng.* **41**(3), 561–566 (2002).
8. B. A. Macintosh et al, "EXtreme Adaptive Optics Planet Imager: overview and status", in *Advancements in Adaptive Optics*. Edited by Domenico B. Calia, Brent L. Ellerbroek, and Roberto Ragazzoni. *Proc. SPIE* **5490**, pp. 359–369 (2004).
9. L. D. Landau and E. M. Lifshitz, *Theory of Elasticity, 3rd Edition*, Course of Theoretical Physics, Volume 7, Pergamon Press, 1986.
10. O. Axelsson and V. A. Barker, *Finite Element Solution of Boundary Value Problems: Theory and Computation*, SIAM, Philadelphia, 2001.
11. Y. Saad, *Iterative Methods for Sparse Linear Systems*, SIAM, Philadelphia, 2003.

List of Figure Captions

Fig. 1. Schematic diagram of Boston Micromachines MEMS deformable mirror.

Fig. 2. Solutions to the actuator equation (6) for (a) the parameter pair $(\rho_i = 20, \nu = 50)$; and (b) the pair $(\rho_i = -10, \nu = 50)$.

Fig. 3. Actuator post displacement plotted against parameters ρ and ν .

Fig. 4. Constant facesheet displacement, or piston, plotted against parameter ν .

Fig. 5. Facesheet response to poked actuators. (a) shows mesh plot of displacement due to a single poked actuator; (b) shows cross section of mesh plot in (a); (c) shows cross sections of the differential displacement from 2 poked actuators and the sum differential displacements from the individual poked actuators.

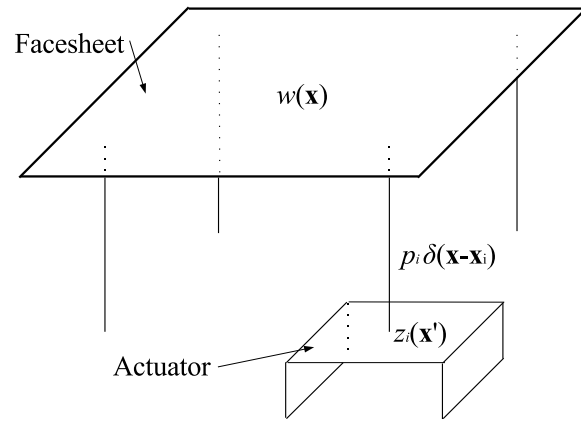


Fig. 1. Schematic diagram of Boston Micromachines MEMS deformable mirror.

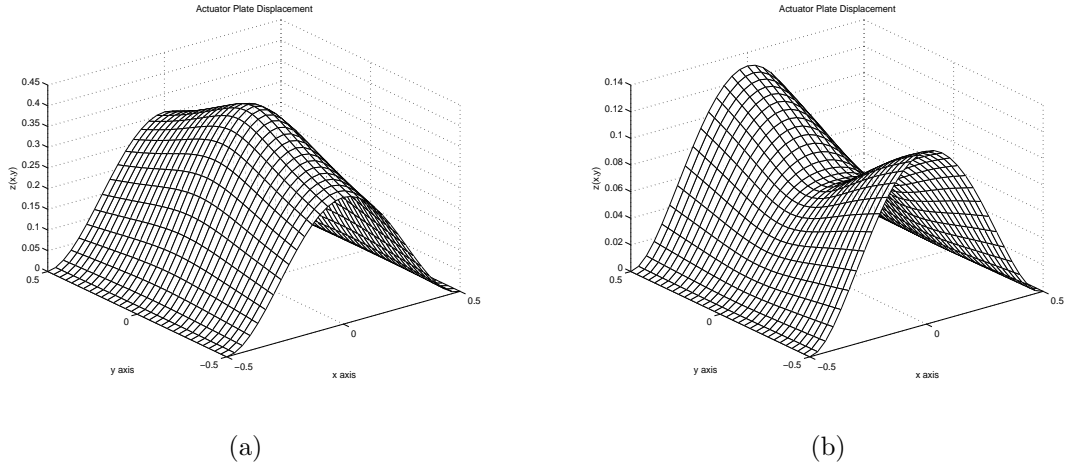


Fig. 2. Solutions to the actuator equation (6) for (a) the parameter pair ($\rho = 20, \nu = 50$); and (b) the pair ($\rho = -10, \nu = 50$).

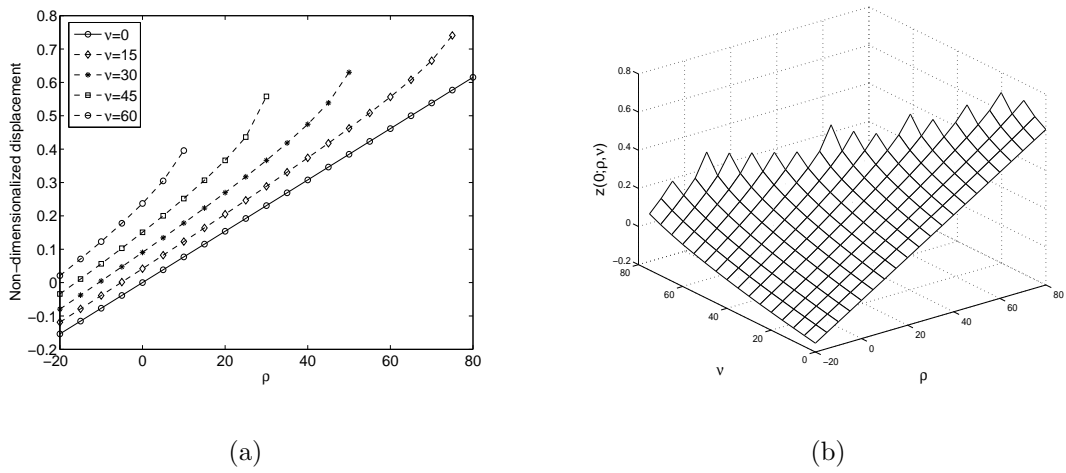


Fig. 3. Actuator post displacement $z(0)$ plotted against parameters ρ and ν .

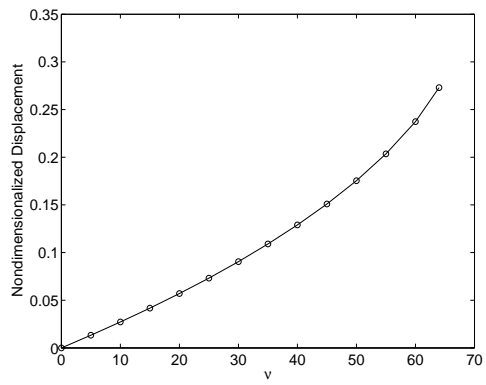


Fig. 4. Constant facesheet displacement, or piston, plotted against parameter ν .

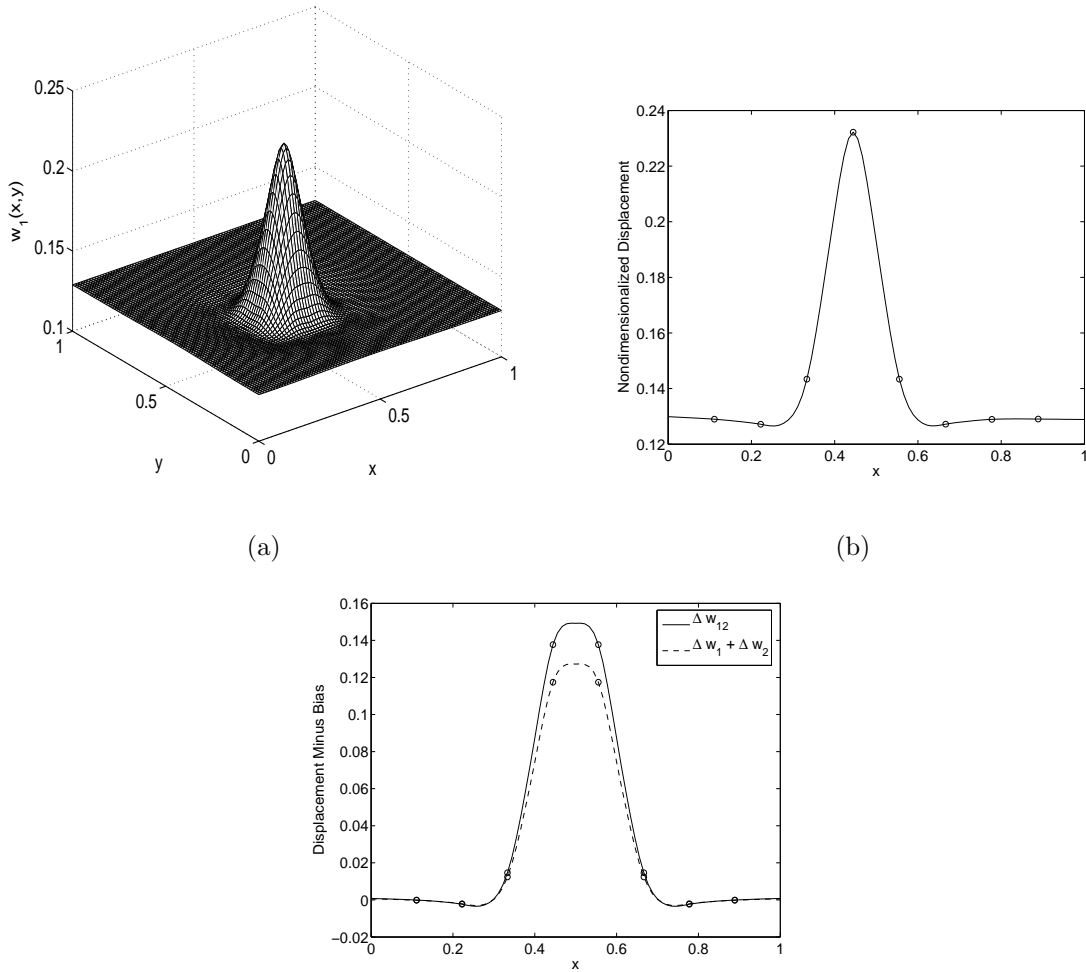


Fig. 5. Facesheet response to poked actuators. (a) shows mesh plot of displacement due to a single poked actuator; (b) shows cross section of mesh plot in (a); (c) shows cross sections of the differential displacement from 2 poked actuators and the sum differential displacements from the individual poked actuators.